



Manuscript received 23 January 2021 Revised manuscript received 12 May 2021 Manuscript accepted 24 May 2021

© 2021 Geological Society of America. For permission to copy, contact editing@geosociety.org

Superhydrous hematite and goethite: A potential water reservoir in the red dust of Mars?

Si Athena Chen¹, Peter J. Heaney¹, Jeffrey E. Post², Timothy B. Fischer³, Peter J. Eng^{4,5} and Joanne E. Stubbs⁴

- Department of Geosciences, The Pennsylvania State University, University Park, Pennsylvania 16802, USA
- ²Department of Mineral Sciences, Smithsonian Institution, Washington, D.C. 20560, USA
- 3Chevron, Houston, Texas 77002, USA
- ⁴Center for Advanced Radiation Sources, The University of Chicago, Chicago, Illinois 60637, USA
- ⁵James Franck Institute, The University of Chicago, Chicago, Illinois 60637, USA

ABSTRACT

Water can be stored in nominally anhydrous minerals as substitutional hydroxyl, generating vast but commonly unrecognized H_2O reservoirs in ostensibly dry regimes. Researchers have long known that hematite $(\alpha\text{-Fe}_2O_3)$ can accommodate small concentrations of hydroxyl through the substitution of Fe³+ by 3H⁺. Our study of natural hematite has demonstrated the occurrence of "hydrohematite" phases that are 10–20 mol% deficient in Fe and accordingly contain 3.6–7.8 mol% structural water. Intergrown with natural hydrohematite samples were superhydrous goethite-like phases exhibiting an Fe deficiency of 10–20 mol% relative to endmember goethite $(\alpha\text{-FeOOH}).$ We synthesized hydrohematite in alkaline solutions (pH 9–12) at low temperatures ($T<200~^\circ\text{C}$) using fresh ferrihydrite as the transient precursor, and we observed a nonclassical crystallization pathway involving vacancy inoculation by Fe as nanocrystals evolved. The high level of incorporation of H_2O in iron (hydr)oxides dramatically alters their behaviors as catalysts and pigments, and the presence of hydrohematite in rocks may rule out high-T diagenesis. We propose that hydrohematite is common in low-T occurrences of Fe oxide on Earth, and by extension it may inventory large quantities of water in apparently arid planetary environments, such as the surface of Mars.

INTRODUCTION

Hematite (Hm, α-Fe₂O₃) and goethite (Gt, α-FeOOH) are common minerals in oxidized terrestrial environments, and they are lowcost materials that are widely used as pigments, electrodes, sorbents, catalysts, etc. (Blake et al., 1966; Giménez et al., 2007; Rovira et al., 2008; Lin et al., 2018). Previous studies have shown that the replacement of <10 mol% Fe by OH modifies the physical and chemical properties of these minerals, generally increasing reactivity and altering the color and magnetic susceptibility (Burgina et al., 2000; Cornell and Schwertmann, 2003; Peterson et al., 2015; Keppeler et al., 2016). In the mid-19th century, mineralogists identified highly Fe-deficient phases based on their unusually bright red streaks, describing them variously as "hydrohematite" or "turgite" (Brush and Rodman, 1867; Pailhé et al., 2008). These mineral species were discredited in the 1920s, however, as being mixtures of endmember Gt and Hm based on primitive powder X-ray diffraction (XRD) data (Posnjak and Merwin, 1922; Böhm, 1925). Studies of the dry thermal dehydration of Gt to Hm inspired efforts to reintroduce the species "hydrohematite" alongside "protohematite" (Wolska, 1981; Dang et al., 1998; Gualtieri and Venturelli, 1999; Burgina et al., 2000).

We document departures from the ideal stoichiometries of Hm and Gt that are too significant to dismiss as minor defect structures. We obtained the original type "hydrohematite" collected by Breithaupt (1847) and compared it with minerals labeled as "turgite" from the Smithsonian National Museum of Natural History (Washington, D.C., USA) and the historic Genth Collection at The Pennsylvania State University (PSU; University Park, Pennsylvania, USA) (Fig. S1A in the Supplemental Material¹). We investigated

the Fe and OH concentrations by electron probe microanalysis (EPMA), Fourier transform infrared spectroscopy (FTIR), thermogravimetric analysis coupled with mass spectrometry (TGA-MS), and Rietveld structure refinements using synchrotron XRD data. We conclude that much of the nodular Hm formed in terrestrial low-temperature environments is better characterized as "hydrohematite". Moreover, we speculate that the spherical hematitic "blueberries" on Mars (Squyres et al., 2004) and perhaps the Hm in Martian dust (Christensen et al., 2001; Fraeman et al., 2013) incorporate hydroxyl, and thus serve as an unappreciated reservoir for water.

IRON DEFICIENCIES AND WATER CONTENTS OF NATURAL HYDROHEMATITE

Electron probe microanalysis of polished sections revealed O/Fe ratios that ranged from 1.88 to 1.74 (± 0.01 ; Table S1), departing markedly from the O/Fe ratio of 1.50 in stoichiometric Fe₂O₃. The total concentration of trace elements was <3 wt% for all specimens, revealing that very little Fe was replaced by impurity elements (e.g., Al, Si, Mg, Mn, and Cr). A broad FTIR peak at 900 cm⁻¹ was prominent in multiple hydrohematite samples but absent in a stoichiometric Hm standard (Fig. 1). This mode at 900 cm⁻¹ is similar to the mode at 890 cm⁻¹ that has been assigned as in-plane deformation (δ_{deform} -OH) vibrations for hydroxyl in Gt (Kustova et al., 1992; Prasad et al., 2006). We also observed broad absorption peaks at 3000–3500 cm⁻¹, attributable to hydroxyl stretching (Prasad et al., 2006). A shift in a band center from 516 cm⁻¹ in stoichiometric Hm to a higher wavenumber

CITATION: Chen, S.A., et al., 2021, Superhydrous hematite and goethite: A potential water reservoir in the red dust of Mars?: Geology, v. 49, p. https://doi.org/10.1130/G48929.1

¹Supplemental Material. Materials, analytical methods, Figures S1–S8, and Tables S1–S3. Please visit https://doi.org/10.1130/GEOL.S.14903316 to access the supplemental material, and contact editing@geosociety.org with any questions.

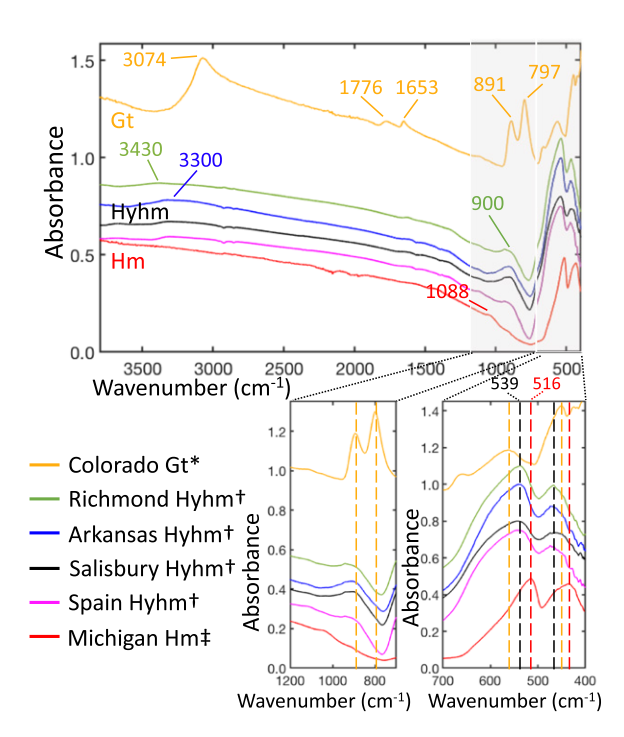


Figure 1. Fourier transform infrared spectroscopy (FTIR) spectra of natural hydrohematite (Hyhm), hematite (Hm), and goethite (Gt). Hyhm has characteristic hydroxyl-related peaks at 900 cm⁻¹ that are not observed in stoichiometric Hm. Broad absorption peak at 3000-3500 cm⁻¹ is due to stretching of hydroxyls. Shift of band center from 516 cm⁻¹ (Hm) to 539 cm⁻¹ (Hyhm) indicates an increase in Fe-OH content, *infrared reference pattern of natural Gt was collected from Colorado, USA (RRUFF™ Project [www. https://rruff.info/1 ID: R050142): †all Hyhm samples were tested in this study (from Richmond. Massachusetts, USA; Arkansas, USA; Salisbury, Connecticut, USA; and Spain); ‡anhydrous Hm was collected from Michigan, USA (RRUFF ID: R040024).

(539 cm⁻¹) in hydrohematite is consistent with an increase in Fe-O bond vibration due to the substitution of OH for O (Ruan et al., 2002). We interpret these results as evidence that the charge deficit generated by missing Fe³⁺ is satisfied by the bonding of H⁺ to octahedral O²⁻. Synchrotron XRD for the hydrohematite samples confirmed that they are monomineralic, showing no impurities of Gt or other Fe hydroxides.

Rietveld analysis of hydrohematite synchrotron XRD patterns (Table S2; Fig. S2) yielded Fe site occupancies that are consistent with the EPMA Fe/O ratios (Table S1). The composition of ideal hydrohematite lies midway between those of Hm and Gt (Fig. 2; Hermann, 1844; Breithaupt, 1847). Assuming a substitution of $3H^+ \leftrightarrow Fe^{3+}$, the general chemical formula of hydrohematite can be expressed as $Fe_{2-x/3}O_{3-x}(OH)_x$ (Wolska, 1981). EPMA analy-

ses of our natural hydrohematite yielded formulae of $Fe_{1.8}O_{2.4}(OH)_{0.6}$ to $Fe_{1.6}O_{1.8}(OH)_{1.2}$ and thus water contents of 3.62-7.80 wt%. Refined Fe site occupancies, equivalent to half the Fe stoichiometry in these formulas, ranged from 0.90 to 0.80 (Fig. 2; Table S3). By comparison, for hydrohematite having a composition equivalent to that of Gt (FeOOH), the Fe occupancy (Fe_{occ}) would be 0.75 with 10.14 wt% H_2O (Fig. 2). Our results therefore confirm the existence of several specimens that are isostructural with Hm (space group $R\overline{3}c$) that have near-goethite water concentrations.

X-ray diffraction and EPMA investigations revealed variations in Fe_{occ} within a single hydrohematite botryoidal specimen. For example, EPMA analyses of hydrohematite from Richmond, Massachusetts (USA), yielded an Fe_{occ} of $0.82~(\pm0.02)$ near the botryoidal ex-

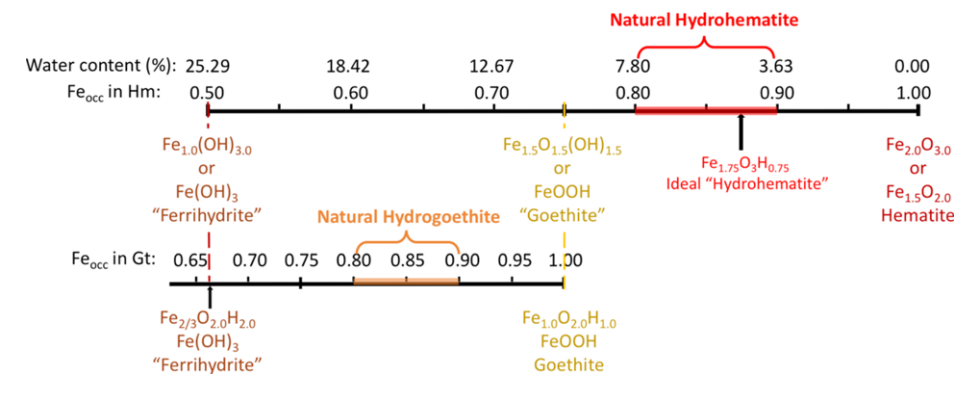


Figure 2. Schematic diagram of chemical composition of natural hydrohematite and hydrogoethite. Fe $_{occ}$ refers to Fe occupancy. Ideal hydrohematite described by Breithaupt and Hermann in the 1840s (Hermann, 1844; Breithaupt, 1847) locates midway between stoichiometric hematite (Hm) and goethite (Gt). The general formula of hydrohematite and hydrogoethite can be represented as Fe $_{2-x/3}O_{3-x}(OH)_x$ and Fe $_{1-y/3}O_{1-y}(OH)_{1+y}$, respectively.

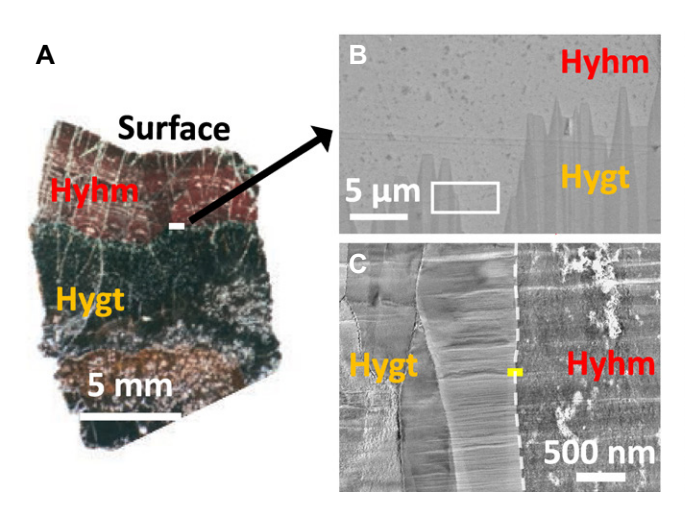
terior and 0.86 (± 0.02) 1.0 cm beneath the surface (Fig. S3). These subtle differences in Fe_{occ} correlated with observed variations in the growth bands in backscattered electron images, with more iron-rich layers appearing relatively brighter (Fig. S3). Similarly, Rietveld refinements using XRD data collected from different regions within a single hydrohematite nodule from Salisbury, Connecticut, yielded a range in Fe_{occ} of 0.82–0.88 (± 0.02) (Fig. S2B; Table S1).

INTERGROWTH OF HYDROHEMATITE AND HYDROGOETHITE

Transmission and scanning electron microscopy of a natural hydrohematite from Arkansas revealed no evidence for intergrowths of ferrihydrite or noncrystalline Fe-hydroxide phases to account for the observed water contents. Images of interior sections of this botryoidal sample revealed an underlying radial fibrosity (Fig. S4), with fibers forming bands or layers oriented perpendicular to the growth direction. High-resolution transmission electron microscopy (HRTEM) of focused ion beam (FIB) sections prepared parallel to the fiber direction revealed that radial fibers were composed of hexagonal nanocrystals measuring ~10 nm in diameter. Lattice fringes were continuous across nanocrystal boundaries within individual fibers, and selected area electron diffraction (SAED) indicated a growth direction parallel to [001] of the hydrohematite nanocrystals. These observations suggest that growth of botryoidal hydrohematite proceeded by topotactic attachment of nanocrystals.

Some hydrohematite samples from Salisbury (Connecticut), Arkansas, and Spain showed intergrowths of Gt (Fig. 3; Fig. S5). EPMA revealed that the Gt also was non-stoichiometric relative to Fe. To our knowledge, natural Gt that is significantly deficient in Fe has not been previously reported, and hereafter we refer to this phase as "hydrogoethite" (Fig. 2). EPMA compositions of hydrogoethite ranged from $Fe_{0.80}O_{0.40}(OH)_{1.60}$ to $Fe_{0.90}O_{0.70}(OH)_{1.30}$ in our samples. Our Rietveld refinements of synchrotron XRD data are consistent with the EPMA results, with refined Fe_{occ} ranging from 0.80 to 0.90 and accordingly calculated water contents from 18.41 to 14.00 wt% in our samples (Fig. S6; Table S4).

High-resolution transmission electron microscopy of the hydrogoethite in a Salisbury sample revealed that radially fibrous monomineralic bands of nanocrystalline hydrogoethite alternate with the monomineralic bands of hydrohematite (Fig. 3). SAED patterns indicated that hydrogoethite fibers grew parallel to the Gt structure c-axis. Moreover, they suggested that the [100] and [010] axes of microcrystalline hydrogoethite (space group Pnma) grew parallel to [001] and [110], respectively, of coexisting cryptocrystalline hydrohematite ($R\overline{3}c$). HRTEM images showed lattice continuity at the interface



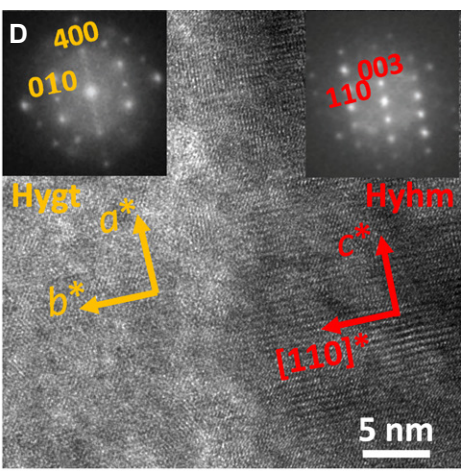


Figure 3. Intergrowth of natural hydrohematite (Hyhm) and hydrogoethite (Hygt) from Salisbury, Connecticut, USA (Genth [Genth Collection at The Pennsylvania State University, USA] specimen #255.3), Images show the interface of Hyhm and Hygt as observed by light reflectance microscopy (A), scanning electron microscopy (B), focused ion beam (FIB)-transmission electron microscopy (TEM) (C), and high-resolution TEM (HRTEM) (D), with two inserted selected area electron diffraction (SAED) patterns of Hyhm

and Hygt. Hyhm and Hygt are seen to grow as separate bands (A). FIB-thinned sample (C) was prepared along the interface (white dashed line in C) between Hygt and Hyhm (white rectangles in A and B). HRTEM of interface (yellow rectangle in C) indicates that Hyhm fibers grew along the c^* axis, and Hygt is epitaxially intergrown with Hyhm such that a^*_{Hygt} is parallel to c^*_{Hyhm} , and b^*_{Hygt} is parallel to [110]* $^*_{\text{Hyhm}}$.

of hydrogoethite and hydrohematite layers. The abrupt transitions between bands of hydrohematite and hydrogoethite, and the monomineralic nature of individual bands, argue against formation of one phase from the other. Rather, we interpret the alternating bands of hydrogoethite and hydrohematite as reflecting different episodes of primary precipitation. As revealed by our laboratory precipitation experiments, described below, small changes in environmental conditions, such as pH, temperature (*T*), Fe activity, etc., can toggle the system between hydrohematite and hydrogoethite generation.

To investigate the thermal stability of hydrohematite from Salisbury (Connecticut), we measured the release of H2O by TGA-MS and separately monitored the change in Fe_{occ} in hydrohematite with increasing T using timeresolved X-ray diffraction (TRXRD). Our TGA-MS experiments revealed episodes of H₂O loss between 120 °C and 200 °C (differential peak at 175 °C) and between 200 °C and 350 °C (peak at 275 °C), suggesting distinct dehydration events for differently bound species of hydroxyl. Total water losses were ~5.2 wt% H₂O (Fig. S7), consistent with a composition halfway between those of Hm (0 wt% H₂O) and Gt (10.14 wt% H_2O) (Fig. 2). We interpret the low-T weight loss (<150 °C) to the desorption of H₂O and/or OH at grain boundaries and dislocations in these highly defective nanocrystals. In situ synchrotron XRD during heating of dry hydrohematite powders showed that hydrohematite started to lose structural hydroxyl above ~150 °C and fully transformed to anhydrous Hm by 700 °C (Fig. S7). Consequently, the presence of hydrohematite in a rock would seem to rule out dry heating over ~300 °C. The OH groups in hydrohematite could not, however, be fully extracted at T < 500 °C (Fig. S7), suggesting that the transformation of hydrohematite to anhydrous Hm requires a high activation energy (Wolska, 1981). Moreover, in contrast to 19th-century reports (Brush and Rodman, 1867), we boiled Salisbury hydrohematite powder at 120 °C for two weeks in deionized water and it did not lead to a conversion to Hm.

FORMATION OF HYDROHEMATITE

In order to determine how the presence of hydrohematite and hydrogoethite might constrain the geologic history of a paleosol or host rock, we investigated the transformation of ferrihydrite (Fh) to Hm ± Gt for a range of solution pH (2–13) and T (70–200 °C) in both batch and in situ synchrotron XRD experiments (Fig. 4) (Heaney et al., 2020). The conversion from Fh is the most common pathway for Hm formation in low-T natural systems (Cornell and Schwertmann, 2003; Lagroix et al., 2016). Although prior researchers have precipitated hydrohematite as a transient intermediate reactant (Peterson et al., 2018), for the first time, we successfully synthesized hydrohematite as a final metastable product from fresh two-line Fh gel. TRXRD revealed that when Fh gels were adjusted to pH 9-12 and heated at moderately low T (80-170 °C), Fe-deficient hydrohematite initially nucleated with Fe_{occ} ~0.50 (Fig. S8). As the crystals grew, the Fe_{cos} increased to, and leveled off at, typical hydrohematite values (Fe $_{occ}$ = 0.80–0.90). For example, at pH 11 and 90 °C, the Fe_{occ} in hydrohematite increased from 0.68 to 0.84 within 0.5 h and remained stable at 0.84 for the remaining 4 h of the experiment (Fig. 4). The decrease in Fe vacancies was accompanied by aggregation and growth of hydrohematite nanoparticles (Waychunas et al., 2005; Niederberger and Cölfen, 2006; Soltis and Penn, 2016). Unlike minerals evolving through classical growth mechanisms that involve the attachment of atoms to the surfaces of stoichiometric crystals, hydrohematite and hydrogoethite evolve through the infilling of interior vacancies via diffusion of surficial

Fe during crystal growth (Fig. S8) (Peterson et al., 2018).

The crystal structure of synthetic hydrohematite prepared at 90 °C for 1 h in a solution initially at pH 11 was virtually identical to that of the natural Hm from Salisbury (Connecticut), both in terms of unit-cell parameters and refined atomic positions (Table S2). Relative to stoichiometric Hm, the higher concentration of Fe vacancies in hydrohematite diminishes the Fe-Fe repulsions, thereby decreasing the octahedral distortion. Additionally, the Fe-O1 bond (the longest Fe-O octahedral bond) in natural hydrohematite is longer than in anhydrous Hm (Table S2), consistent with a model in which H preferentially bonds with the O1 anions, resulting in a longer Fe-OH bond (Fig. 4).

GEOLOGICAL SIGNIFICANCE

Our examination suggests that hydrous and Fe-deficient iron oxides are surprisingly common; we observed hydrohematite as a primary mineral within sedimentary rocks alongside quartz and clays. We propose that many terrestrial radially fibrous Fe-oxide nodules in fact consist of these superhydrous phases, such as the red ochres used by early hominids for pigmentation. If so, then Fe-oxide concretions observed on nominally dry planets, such as the hematitic concretions ("blueberries") in Meridiani Planum on Mars, may serve as an unrecognized reservoir for water (Squyres et al., 2004). We note that a 1-cm-thick layer of hydrohematite enveloping a Mars-sized planet would sequester a volume of water equivalent to 4.32×10^{11} m³, or roughly the amount in Lake Erie (northeastern North America). Our results also indicate that these superhydrous phases can survive without diagenetic alteration to end-member Hm for long durations. The hydrohematite and hydrogoethite from Salisbury (Connecticut), studied here were located in the major iron-ore district that was active in that

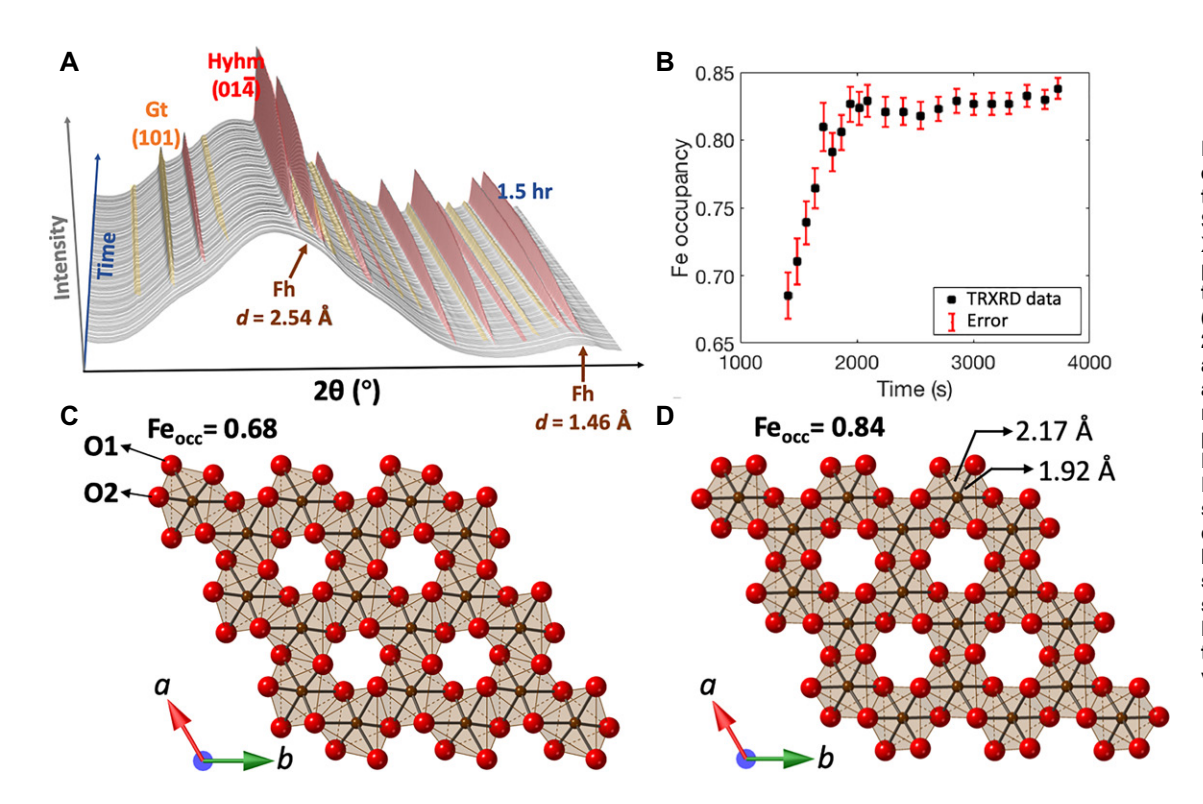


Figure 4. Crystallographic evolution of hydrohematite (Hyhm) formation. (A) Stacked time-resolved X-ray diffraction (TRXRD) patterns of transformation of two-line ferrihydrite (Fh, with d-spacings [d] at 2.54 Å and 1.46 Å) to Hyhm and goethite (Gt) at 90 °C and pH 11. (B) Rietveld refinement of Fe occupancy (Fe_{occ}) for synthetic Hyhm revealed an initial $Fe_{occ} = 0.68$. Errors represent estimated standard deviations as calculated by GSAS-II. (C,D) Hyhm structure evolved from structure with high (C) to low (D) octahedral distortion with increasing vacancy inoculation.

area from 1732 to 1904. These iron (hydr)oxides occur on an unconformity between the underlying Cambrian-Ordovician Stockbridge Marble and the overlying Ordovician Walloomsac Schist, and they are interpreted as a metamorphosed lateritic paleosol horizon (Hobbs, 1907). Consequently, hydrohematite and hydrogoethite likely persisted at this site for several hundred million years, indicating a high degree of metastability. This study promises geochemical constraints for the formation and heating histories for terrestrial and planetary rocks that contain these phases.

ACKNOWLEDGMENTS

We thank Katherine Crispin of the Penn State Materials Characterization Laboratory (The Pennsylvania State University, USA) for her generous help and suggestions with EPMA data collection. In addition, Trevor Clark, Haiying Wang, and Ke Wang assisted with FIB sample preparation and transmission electron microscopy data collection. We thank Florence T. Ling for collecting FTIR data for Hm at the Smithsonian Institution (Washington, D.C., USA), and Xin Gu for discussions of geochemistry. We are grateful to Andreas Massanek of the Technische Universität Bergakademie (Freiberg, Germany) for sharing a sample of the "type" hydrohematite collected by J.F.A. Breithaupt in 1843. This work was funded by a seed grant from the Pennsylvania State University Biogeochemistry dual-title Ph.D. program and by U.S. National Science Foundation (NSF) grants EAR-1552211 and EAR-1925903. Synchrotron XRD was measured at GeoSoilEnviroCARS (The University of Chicago, Sector 13), Advanced Photon Source (APS), Argonne National Laboratory (ANL). GeoSoilEnviroCARS is supported by the NSF-Earth Sciences (grant EAR-1634415) and U.S. Department of Energy (DOE)-GeoSciences (grant DE-FG02-94ER14466). The APS is a DOE Office of Science User Facility operated by ANL under Contract No. DE-AC02-06CH11357.

REFERENCES CITED

Blake, R.L., Hessevic, R.E., Zoltai, K.T., and Finger, L.W., 1966, Refinement of the hematite structure: American Mineralogist, v. 51, p. 123–129.

Böhm, J., 1925, Über Aluminium- und Eisenhydroxyde I: Zeitschrift für Anorganische und Allgemeine Chemie, v. 149, p. 203–216, https://doi.org/10.1002/zaac.19251490114.

Breithaupt, J.F.A., 1847, Vollständiges Handbuch Der Mineralogie, Vol. 3: Dresden, Leipzig, Arnoldische Buchhandlung.

Brush, G.J., and Rodman, C.S., 1867, Contributions from the Sheffield Laboratory of Yale College. No. XV: Observations on the native hydrates of iron: American Journal of Science and Arts (1820–1879), v. s2-44, p. 219–222, https://doi.org/10.2475/ajs.s2-44.131.219.

Burgina, E.B., Kustova, G.N., Tsybulya, S.V., Kryukova, G.N., Litvak, G.S., Isupova, L.A., and Sadykov, V.A., 2000, Structure of the metastable modification of iron(III) oxide: Journal of Structural Chemistry, v. 41, p. 396–402, https://doi.org/10.1007/BF02741997.

Christensen, P.R., Morris, R.V., Lane, M.D., Bandfield, J.L., and Malin, M.C., 2001, Global mapping of Martian hematite mineral deposits: Remnants of water-driven processes on early Mars: Journal of Geophysical Research, v. 106, p. 23,873– 23,885, https://doi.org/10.1029/2000JE001415.

Cornell, R.M., and Schwertmann, U., 2003, The Iron Oxides. Structures, Properties, Reactions, Occurences and Uses (second edition): Weinheim, Germany, Wiley, 664 p., https://doi.org/10.1002/3527602097.

Dang, M., Rancourt, D.G., Dutrizac, J.E., and Lamarche, G., 1998, Interplay of surface conditions, particle size, stoichiometry, cell parameters, and magnetism in synthetic hematite-like materials: Hyperfine Interactions, v. 117, p. 271–319, https://doi.org/10.1023/A:1012655729417.

Fraeman, A.A., et al., 2013, A hematite-bearing layer in Gale Crater, Mars: Mapping and implications for past aqueous conditions: Geology, v. 41, p. 1103–1106, https://doi.org/10.1130/G34613.1.

Giménez, J., Martínez, M., de Pablo, J., Rovira, M., and Duro, L., 2007, Arsenic sorption onto natural hematite, magnetite, and goethite: Journal of Hazardous Materials, v. 141, p. 575–580, https://doi.org/10.1016/j.jhazmat.2006.07.020.

Gualtieri, A.F, and Venturelli, P., 1999, In situ study of the goethite-hematite phase transformation by real time synchrotron powder diffraction: American Mineralogist, v. 84, p. 895–904, https://doi.org/10.2138/am-1999-5-625.

Heaney, P.J., Oxman, M.J. and Chen, S.A., 2020, A structural study of size-dependent lattice variation: In situ X-ray diffraction of the growth of goethite nanoparticles from 2-line ferrihydrite: American Mineralogist, v. 105, p. 652–663, https://doi.org/10.2138/am-2020-7217.

Hermann, R., 1844, Untersuchungen russischer Mineralien: Journal für Praktische Chemie, v. 33, p. 282–300, https://doi.org/10.1002/ prac.18440330139.

Hobbs, W.H., 1907, The iron ores of the Salisbury District of Connecticut, New York, and Massachusetts: Economic Geology and the Bulletin of the Society of Economic Geologists, v. 2, p. 153–181, https://doi.org/10.2113/gsecongeo.2.2.153.

Keppeler, M., Shen, N., Nageswaran, S., and Srinivasan, M., 2016, Synthesis of α-Fe₂O₃/carbon nanocomposites as high capacity electrodes for next generation lithium ion batteries: A review: Journal of Materials Chemistry: A, Materials for Energy and Sustainability, v. 4, p. 18,223–18,239, https://doi.org/10.1039/C6TA08456G.

Kustova, G.N., Burgina, E.B., Sadykov, V.A., and Poryvaev, S.G., 1992, Vibrational spectroscopic investigation of the goethite thermal decomposition products: Physics and Chemistry of Minerals, v. 18, p. 379–382, https://doi.org/10.1007/BF00199419.

Lagroix, F., Banerjee, S.K., and Jackson, M.J., 2016, Geological occurrences and relevance of iron oxides, *in* Faivre, D., ed., Iron Oxides: From Nature to Applications: Weinheim, Germany, Wiley, p. 9–29, https://doi.org/10.1002/9783527691395.ch2.

Lin, X., Heaney, P.J., and Post, J.E., 2018, Iridescence in metamorphic "rainbow" hematite:

- Gems & Gemology, v. 54, p. 28–39, https://doi.org/10.5741/GEMS.54.1.28.
- Niederberger, M., and Cölfen, H., 2006, Oriented attachment and mesocrystals: Non-classical crystallization mechanisms based on nanoparticle assembly: Physical Chemistry Chemical Physics, v. 8, p. 3271–3287, https://doi.org/10.1039/B604589H.
- Pailhé, N., Wattiaux, A., Gaudon, M., and Demourgues, A., 2008, Impact of structural features on pigment properties of α-Fe₂O₃ haematite: Journal of Solid State Chemistry, v. 181, p. 2697–2704, https://doi.org/10.1016/j.jssc.2008.06.049.
- Peterson, K.M., Heaney, P.J., Post, J.E., and Eng, P.J., 2015, A refined monoclinic structure for a variety of "hydrohematite": American Mineralogist, v. 100, p. 570–579, https://doi.org/10.2138/ am-2015-4807.
- Peterson, K.M., Heaney, P.J., and Post, J.E., 2018, Evolution in the structure of akaganeite and hematite during hydrothermal growth: An in situ synchrotron X-ray diffraction analysis: Powder Diffraction, v. 33, p. 287–297, https://doi .org/10.1017/S0885715618000623.

- Posnjak, E., and Merwin, H., 1922, Additions and corrections—The system, Fe₂O₃-SO₃-H₂O: Journal of the American Chemical Society, v. 44, 2969, https://doi.org/10.1021/ja01433a610.
- Prasad, P.S.R., Shiva Prasad, K., Krishna Chaitanya, V., Babu, E.V.S.S.K., Sreedhar, B., and Ramana Murthy, S., 2006, In situ FTIR study on the dehydration of natural goethite: Journal of Asian Earth Sciences, v. 27, p. 503–511, https://doi .org/10.1016/j.jseaes.2005.05.005.
- Rovira, M., Giménez, J., Martínez, M., Martínez-Lladó, X., de Pablo, J., Martí, V., and Duro, L., 2008, Sorption of selenium(IV) and selenium(VI) onto natural iron oxides: Goethite and hematite: Journal of Hazardous Materials, v. 150, p. 279–284, https://doi.org/10.1016/ j.jhazmat.2007.04.098.
- Ruan, H.D., Frost, R.L., Kloprogge, J.T., and Duong, L., 2002, Infrared spectroscopy of goethite dehydroxylation: III. FT-IR microscopy of in situ study of the thermal transformation of goethite to hematite: Spectrochimica Acta, Part A: Molecular and Biomolecular Spectroscopy, v. 58,

- p. 967–981, https://doi.org/10.1016/S1386-1425(01)00574-1.
- Soltis, J.A, and Penn, R.L., 2016, Oriented attachment and nonclassical formation in iron oxides, in Faivre, D., ed., Iron Oxides: From Nature to Applications: Weinheim, Germany, Wiley, p. 243–68, https://doi.org/10.1002/9783527691395.ch11.
- Squyres, S.W., et al., 2004, In situ evidence for an ancient aqueous environment at Meridiani Planum, Mars: Science, v. 306, p. 1709–1714, https://doi.org/10.1126/science.1104559.
- Waychunas, G.A., Kim, C.S., and Banfield, J.F., 2005, Nanoparticulate iron oxide minerals in soils and sediments: Unique properties and contaminant scavenging mechanisms: Journal of Nanoparticle Research, v. 7, p. 409–433, https://doi .org/10.1007/s11051-005-6931-x.
- Wolska, E., 1981, The structure of hydrohematite: Zeitschrift für Kristallographie—New Crystal Structures, v. 154, p. 69–75, https://doi.org/10.1524/zkri.1981.154.1-2.69.

Printed in USA